Journal of Structural Geology, Vol. 14, No. 8/9, pp. 893 to 903, 1992
Printed in Great Britain

0191-8141/92 $05.00+0.00

Kinetic instabilities during the propagation of a branch crack: effects of loading conditions and internal pressure

M. BARQUINS

Laboratoire de Physique et Mécanique des Milieux Hétérogènes, URA au CNRS No. 857, ESPCI, 10 rue Vauquelin, 75231 Paris Cédex 05, France

and

J.-P. PETIT

Laboratoire de Géologie Structurale, URA au CNRS No. 1371 USTL, Place E. Bataillon, 34095 Montpellier Cédex 5, France

(*Received* 3 *October* 1991; *accepted in revised form* 19 *April* 1992)

Abstract—In order to understand the physical processes controlling the formation of various branch features stemming from pre-existing defects in rocks, this paper presents a model based on fracture mechanics concepts. We examine the consequences of the elastic stress field around an open oblique elliptical defect subjected to constant uniaxial or biaxial stress on the kinetics of the classical branch crack. Assuming that propagation does not fundamentally change the elastic stress field, the strain energy release rate, G, is computed for each branch crack length, L, by integrating the values of the principal stress acting perpendicular to the stress trajectory of the other principal stress, starting exactly from the point of maximum tensile stress at the edge of the elliptical defect. The propagation regime depends on the slope of the $G(L)$ curve and on its position with respect to the equilibrium value G_o and the critical value G_c, for which catastrophic rupture occurs.

Without internal pressure, the unimodal curves predict three possible successive propagation regimes: (1) stable propagation with increasing velocity; (2) catastrophic propagation with velocity jump and associated acoustic emission; and (3) stable propagation with decreasing velocity. The catastrophic regime is limited to high load values. Experimentally, the triggering of the propagation can be very difficult to predict, as it depends on slight variations in the length of pre-existing microcracks stemming from the elliptical defect at the root of the branch crack path.

With internal pressure, the stress field is modified so that the maximum tensile stress is present at some distance from the edge of the elliptical defect. This can result in a change in the shape of $G(L)$ curves which indicates that two independent velocity jumps may occur: the first one is mainly linked to the local influence of the defect, the second (leading to a large extension) is due to the general influence of the internal pressure.

INTRODUCTION

THE most widespread mechanism for fault development is the extension of pre-existing defects of whatever origin, for these act as stress concentrators. This development can occur through the connection of individual faults which can be considered as elementary faults (Granier 1985). They can extend, either by shear neo-rupture at the tips of pre-existing defects in confined conditions (relatively high lateral stress), or by branch features developing in Mode I (opening mode) at a high angle with respect to the oblique defect, and with low lateral stress (Petit & Barquins 1987). Thus it is absolutely essential to have an accurate physical basis to understand the behaviour of such fractures. This implies a fracture mechanics approach (Lawn & Wilshaw 1975). It may include not only the complete definition of the associated stress and displacement field which gives insight into the kinematics of faulting (Pollard & Segall 1987) but also the physical definition of initiation and propagation conditions. A kinetic approach to branching development is essential to understand propagation; this is the aim of this paper.

Geological branch features formed at the tips of pre-existing joints subjected to shearing movements can be of various types. Figure 1 shows a few classical field examples on different scales, such as fault–stylolite–tension gash structures (Rispoli 1981) branching perpendicular to a fault in limestone, and horse tail fractures in granite (Granier 1985). The most important physical conditions controlling the formation of such features for a given rock are the remote stresses, in particular the values and ratio of the two main principal stresses, the orientation, size and shape of the defect, and the internal fluid pressure which can play an important part in joint or fault reactivation (Sibson 1990) and extension (Pollard 1973, Engelder & Lacazette 1990).

All these factors can influence the path and kinetics of branching. An important aim is to determine whether these features are related to a catastrophic (seismic) movement or to slower (subcritical) movement.

The physical approach presented here is based on: (i) experiments; and (ii) analytical study of the stress field around an elliptical open defect subjected to uniaxial loading with or without superimposition of lateral confinement and/or internal pressure; the corresponding stress fields form a basis for fracture mechanics derivations. The propagation kinetics are studied in terms of strain energy release rate, G, which allows us to predict the different types of propagation regimes: stable and

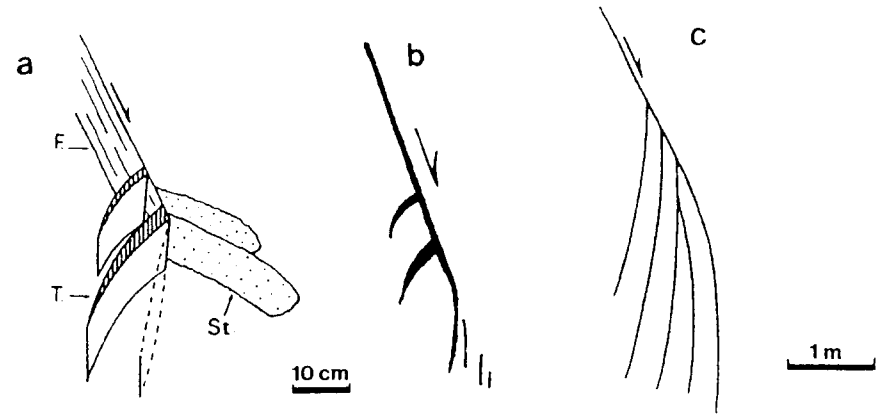

Fig. 1. Examples of branching structures. (a) Faults (F), stylolite (St), tension gashes (T) in Languedoc limestone; (b) orthogonal branching of a calcite vein in Col du Lautaret limestone (French Alps); (c) horse tail fractures corresponding to the damping of a strike slip fault reactivated from a joint in granite (Granier 1985).

Table 1. Equilibrium and propagation regimes: terminology

$G = G_0$ and $\partial G/\partial L < 0$	stable equilibrium
$G = G_0$ and $\partial G/\partial L > 0$	unstable equilibrium
$G_0 > G > G_c$ and $\partial G/\partial L > 0$	stable propagation at increasing speed; i.e. it is not necessary to increase the load to accelerate the crack propagation; the corresponding regime is called 'spontaneous'
$G_0 > G > G_c$ and $\partial G/\partial L < 0$	stable propagation at decreasing speed; i.e. a continuous propagation would require an increase in load; the corresponding regime is called 'controllable'
$G = G_c$	unstable propagation with acoustic emission due to a velocity jump, this propagation cannot be influenced at all; the corresponding regime is called 'catastrophic'

L is the length of the initial microcrack or of the branch crack.
G_0 is the strain energy release rate at the equilibrium (zero crack propagation speed).
G_c is the strain energy release rate corresponding to the appearance of a velocity jump.

'spontaneous' (increasing crack speed), stable and 'controllable' (decreasing crack speed) or 'catastrophic' (velocity jumps), and their chronological appearance. The three terms in inverted commas are defined in Table 1. Here the kinetics of the branch crack under uniaxial and biaxial loading conditions are presented, and then the role of internal pressure on the initiation and extension of the branch crack for both situations is investigated. This complete and detailed study of the possible behaviour of an isolated defect differs from the work of Nemat-Nasser & Horii (1982) and Ashby & Hallam (1986) which dealt with a single defect submitted to increasing loading, in order to study the possible interaction of several defects at various distances apart.

UNIAXIAL LOADING CONDITIONS

The path and kinetics of branch crack propagation were studied using Plexiglas® (PMMA, polymethylmethacrylate) plates (50 × 32 × 5 mm), each with a 0.3 mm wide and 10 mm long slot oriented in various directions with respect to the loading axis (angle β). In these experiments, the long edges of the Plexiglas plates were inserted without friction in grooved beams, in order to avoid buckling, and were submitted to a given level of uniaxial loading parallel to the main axis of the plate by means of a servo-controllable hydraulic device. Thus, deformation and rupture occurred under constant load (as in creep testing but under compression).

Under moderate uniaxial constant loading conditions compatible with purely brittle deformation, Mode 1 (opening mode) propagation of the branch crack occurred in the Plexiglas sample (Fig. 2a). Such structures have already been observed by other authors in various brittle or semi-brittle materials: in glass (Brace & Bombolakis 1963, Hoek & Bienawsky 1965, Cottrell 1972, Sketty *et al.* 1987), in plaster (Lajtai 1971) and in polymers (Nemat-Nasser & Horii 1982, Ashby and Hallam 1986). However, we also demonstrated that propagation was followed at higher stress levels by the formation of a shear band, more or less as an extension of the initial defect, which represents a potential propagation path for rupture (Petit & Barquins 1988).

As soon as constant axial stress was applied, we observed that a branch fracture appeared in the slot tip vicinity initiated from one of the many microcracks induced by the sawing of the slot. Simultaneously, or after a few seconds, a second branch fracture developed at the other tip, as observed by Cottrell (1972). Both cracks then propagated along trajectories which curved more or less according to the initial slot angle β (angle between slot and loading axis), but remained perfectly centro-symmetric (Fig. 2a). Whatever the initial slot angle, branching was always perpendicular to the local tangent at the slot edge from a point whose distance to the slot tip increases with increasing β. Figure 3 illustrates the branching for $\beta = 15°$, 45° and 75°.

The analytical model is based on the following assumptions: the slotted Plexiglas sample is assimilated to an infinite plate including an elliptical hole whose long axis $2a$ is equal to the length of the slot and with short axis $2b$, where b is deduced from the radius of curvature R of the slot tips ($R = b^2/a = 0.15$ mm). A classical

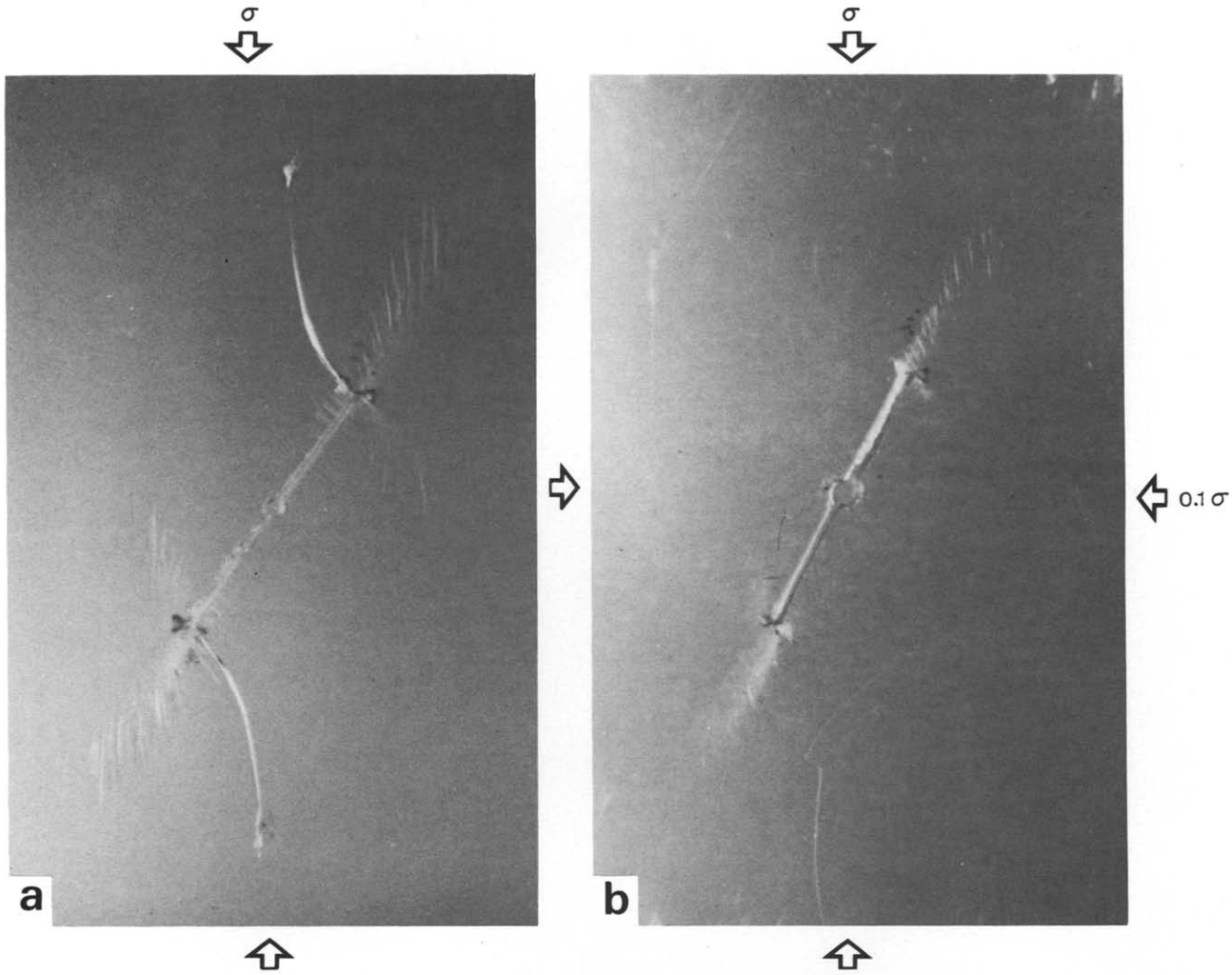

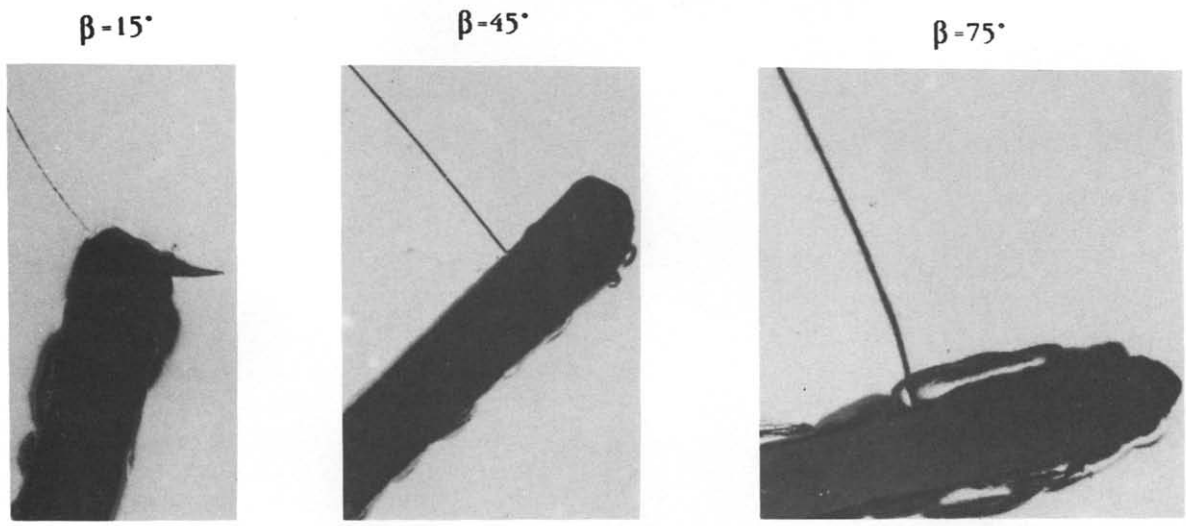

Fig. 2. (Top.) Plexiglas plate after testing. (a) Uniaxial loading with two symmetrical branch cracks; (b) biaxial loading without a branch crack but with a shear band outlined by en échelon shallow microcracks ($\beta = 30°$, $a = 8$ mm, $R = 150\,\mu$m).

Fig. 3. (Bottom.) Microscopic view of the root of a branch crack observed for an uniaxial compressive load applied to Plexiglas plates for $\beta = 15°$, 45° and 75° ($a = 5$ mm, $r = 150\,\mu$m).

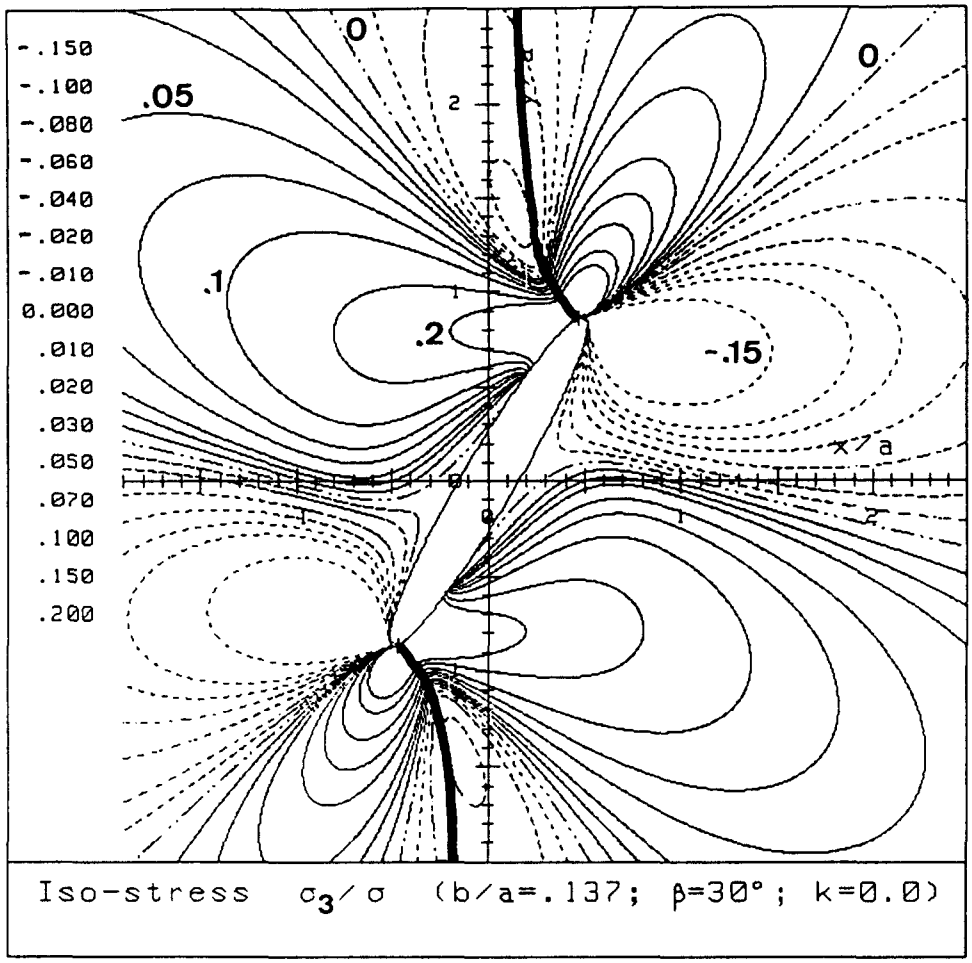

Fig. 4. Calculated contours of the principal stress σ_3 around an elliptical slot ($b/a = 0.137$) inclined at $\beta = 30°$ to the uniaxial loading axis. Unbroken lines are contours corresponding to tensile stress (with positive values); broken lines to compressive stress (with negative values). These values (given in the lateral column or by bold numbers on some of the contours) are normalized by the absolute value of the applied compressive stress σ ($a = 8$ mm, $R = 150\,\mu$m). The superimposed bold lines are the stress trajectories of σ_1 starting from the point where the tensile stress σ_3 is maximum at the edge of the elliptical slot. This trajectory predicts the potential path of the branch crack.

system of curvilinear co-ordinates defined by two families of confocal ellipses and hyperboles was used so that the foci were the same as the ellipse representing the slot. Hence the Kolosov–Muskhelishvili (Muskhelishvili 1975) formalism allows us to express the stresses on a smaller experimental volume (Pollard 1973, Wu & Chang 1978, Barquins *et al.* 1989a). Figure 4, for instance, shows the contours of σ_3, the minimum principal stress (normalized to the applied axial constant stress σ), with superimposition of the trajectory of the maximum principal stress σ_1, branching from the edge of the elliptical defect at the point of the maximum (tensile) σ_3 value. This stress field analysis completely bears out the observations that the branch fracture is not initiated at the extreme tip of the slot but at a distance from it which increases with increasing angle to loading β (Fig. 3). This confirms the pioneering statement of Inglis (1913) that the important parameter is not the slot width but the radius of curvature at the tips. The model also confirms that the branch crack is initiated at the point of the slot edge where the tensile stress is maximum and that the branch crack propagates along the trajectory of σ_1 at this point.

The propagation kinetics of the branch crack have been studied in terms of strain energy release rate, G. Here we briefly recall the basis for the construction and analysis of the $G(L)$ curves; more details will be found in Barquins *et al.* (in press).

Two symmetrical branch cracks with the common length L can be considered as a single rectilinear crack with the length $2L$, assuming that propagation does not fundamentally change the elastic stress field. We follow the methods used by Mouginot & Maugis (1985) to study the Hertzian fracture, and calculate the stress intensity factor K_I according to Paris & Sih (1965) by integrating the principal stress σ_3 along the branch crack of length L, i.e. along the σ_1 stress trajectory:

$$K_I = 2(L/\pi)^{1/2} \int_0^L [\sigma_3(s)/(L^2 - s^2)^{1/2}]\, ds, \qquad (1)$$

where s is the curvilinear abscissa of the point where the stress $\sigma_3(s)$ is considered. As the plane strain condition is reached as for any three-dimensional crack (in a thick plate), the plane strain formula can be applied to calculate the strain energy release rate G, such as:

$$G = K_I^2(1 - \nu^2)/E, \qquad (2)$$

where E and ν are, respectively, the Young's modulus

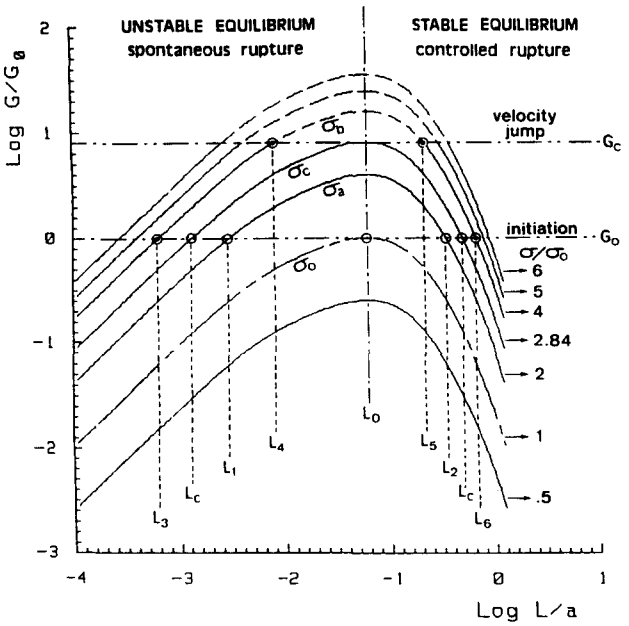

Fig. 5. Calculated variations of the strain energy release rate G (normalized by the strain energy release rate G_0 at zero crack propagation speed) as a function of the length L of a branch crack (normalized by the half-crack length a) along the stress trajectory of σ_1, starting from the point of maximum tensile stress σ_3 at the edge of the slot. The different curves are drawn for various uniaxial applied compressive stress σ normalized by the stress σ_0 whose maximum value is reached for $G = G_0$ ($\beta = 30°$, $a = 8$ mm, $R = 150\,\mu$m).

and the Poisson ratio of the tested elastic body (for Plexiglas, $E = 2.8$ GPa and $\nu = 0.4$).

From this the variations of G as a function of the pre-existing microcrack or branch crack length, L, are calculated and drawn in log–log co-ordinates. Figure 5 corresponds to the experimental conditions ($a = 8$ mm, $R = 150\ \mu$m, $\beta = 30°$) taking into account the value $K_{I0} = 0.66$ MPa.m$^{1/2}$ corresponding to the equilibrium state of a crack (zero crack propagation speed) in Plexiglas (Williams 1972). Starting from equation (2) the values of G are calculated and normalized by $G_0 = 126$ J.m^{-2} corresponding to K_{I0}.

The microcrack or branch crack length L is normalized to the half-length a of the slot. Calculation is presented for various imposed uniaxial loadings σ, the latter being normalized by the stress σ_0, corresponding to the curve in Fig. 5 with maximum amplitude $G/G_0 = 1$. All the curves pass through a maximum value at the same abcissa, L_0 ($L_0 \cong 500\ \mu$m in Fig. 5). This length, L_0, delimits areas of unstable $[(\partial G/\partial L)_\sigma > 0]$ and stable $[(\partial G/\partial L)_\sigma < 0]$ equilibrium states, along the line $G = G_0$. As shown by Williams (1972), as soon as $K_I > K_{I0}$ (i.e. $G > G_0$), a crack is initiated and it propagates with an increasing speed for increasing K_I or G; and conversely, with a decreasing speed if G decreases as the crack grows. Thus, the critical length L_0 also delimits spontaneous rupture $[(\partial G/\partial L)_\sigma > 0]$ with a continuous increasing crack speed, and controllable rupture $[\partial G/\partial L)_\sigma < 0]$ with a decelerating crack speed (see Table 1 for terminology).

Figure 5 predicts the evolution of a pre-existing microcrack at the slot edge according to the length L of this microcrack and the intensity of the applied uniaxial load σ. Let us consider σ_0 the critical load ($\sigma_0 \cong 18$ MPa), with its corresponding curve just reaching (tangentially) the line $G/G_0 = 1$. If $\sigma < \sigma_0$ whatever the microcrack length L, propagation cannot occur and the pre-existing crack tends to close. For $\sigma > \sigma_0$, the corresponding curve (e.g. σ_a in Fig. 5), intersects the equilibrium line for crack lengths L_1 and L_2, distributed on both sides of the value L_0. In this case, only a crack of length L such as $L_1 < L < L_2$ can propagate at constant applied stress σ. If $L_0 < L < L_2$, as the curve slope is negative, the crack grows with a continuously decreasing propagation speed until the equilibrium length L_2 is reached. On the other hand, if $L_1 < L < L_0$, the initiation occurs in an unstable equilibrium area, so that the crack length increases first with an increasing speed up to $L = L_0$ then with a decreasing speed until the same equilibrium value L_2 is reached. The smaller the length of the pre-existing crack, which is placed at the slot edge, the higher the applied stress necessary to initiate the branch crack, and the greater the total length reached at the equilibrium.

As shown above, if $L < L_0$, as soon as G reaches G_0 by increasing the loading σ, a branch crack is initiated and grows at increasing propagation speed because G increases. But it is well known that G cannot exceed the critical value G_c, at which a velocity jump (catastrophic propagation) is observed with an associated acoustic emission. According to Williams (1972) the critical stress intensity factor K_{Ic}, characteristic of Plexiglas, is equal to 1.7 MPa.m$^{1/2}$, so that the corresponding value of G_c is about 1000 J.m^{-2}. Hence, a new critical loading σ_c ($\cong$51 MPa in Fig. 5) can be defined with its corresponding curve just reaching the line $G = G_c$. This curve σ_c intersects the equilibrium line $G = G_0$ at abcissas $L = L_c$ and $L = L'_c$ ($L_c \cong 10\,\mu$m and $L'_c \cong 4$ mm in Fig. 5), so that it can be predicted that the growth of a pre-existing microcrack of length $L < L_c$ must lead to a velocity jump if an adequate loading $\sigma > \sigma_c$ is applied. For instance, let us consider a pre-existing microcrack of length L_3 ($\cong 5\ \mu$m in Fig. 5); as soon as the compressive loading σ_b (corresponding to about 70 MPa) is applied, the length grows at increasing propagation speed along the curve σ_b until the value L_4 ($\cong 64\ \mu$m in Fig. 5) is reached ($G = G_c$). At that moment, a velocity jump of the order of $V_c = 2.5$ cm s^{-1} (Williams 1972) is observed at a nearly constant G, so that the crack length instantaneously acquires a value which cannot be less than L_5 ($\cong$1.7 mm in Fig. 5), though it cannot be exactly predicted. The crack will continue to propagate or will close, according to whether this length corresponds to $G > G_0$ or to $G < G_0$, until a new equilibrium is reached for L_6 ($\cong$5.4 mm). For an increase in the applied loading the new propagation will occur in stable conditions along the equilibrium line $G = G_0$ and a very long branch crack can be obtained.

In order to verify the validity of the predicted different crack propagation régimes, Plexiglas plates with a 0.3 mm wide and 10 mm long central slot orientated at $\beta = 45°$ to the loading axis were submitted to a constant uniaxial compressive stress $\sigma = 35$ MPa which is ade-

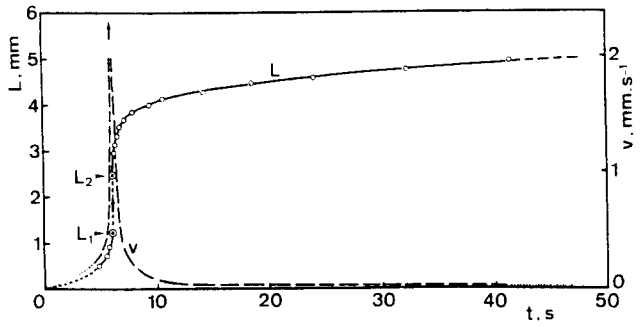

Fig. 6. Length and corresponding propagation speed vs time for a branch crack formed at the tip of a pre-existing oblique open slot in a Plexiglas plate submitted to uniaxial loading ($\beta = 45°$, $a = 5$ mm, $R = 150\,\mu$m, $\sigma = 35$ MPa).

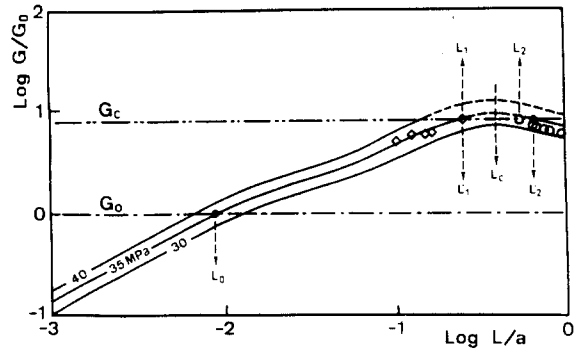

Fig. 8. Strain energy release rate vs branch crack length, in reduced co-ordinates. The curves correspond to the theoretical model; diamonds and circles are experimental data deduced from Figs. 6 and 7.

quate to induce branching from one of the pre-existing microcracks made by the sawing at the slot edge. A typical evolution of the branch crack length L and the associated speed $V = dL/dt$ is shown in Fig. 6. The crack length increased first with an increasing propagation speed until the value $L_1 = 1.25$ mm was reached, then a velocity jump was observed from L_1 to $L_2 = 2.5$ mm with an associated acoustic emission, characteristic of the catastrophic propagation. This velocity jump was followed by a growth of the crack with a decreasing speed until an equilibrium value was reached for L not smaller than 5 mm. This is qualitatively in accordance with the behaviour predicted from Fig. 5 when a constant uniaxial stress such as σ_b is applied to the Plexiglas plate.

As the branch crack experimental configuration did not provide the evolution of G vs the instantaneous speed of the branch crack, this was obtained indirectly in two stages: (i) experimental curves for G as a function of crack speed in opening Mode I were obtained by a classical SDCB (Slotted Double-Cantilever Beam) experiment in Plexiglas; (ii) as the strain energy release rate, G-crack speed relation is the same in both SDCB and branch crack experiments, a value for G can thus be given for each branch crack speed (or corresponding length). The variation of the strain energy release rate G_{SDCB} as a function of the crack propagation speed $v = dL/dt$ is shown in Fig. 7. The crack propagation speeds given in Figs. 5 and 6 allow us to associate every branch crack length L to a corresponding strain energy release rate G (Barquins *et al.* 1989b).

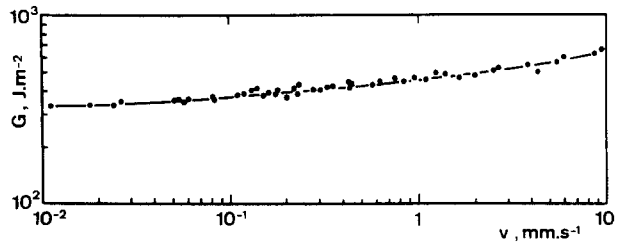

Fig. 7. Strain energy release rate vs corresponding crack propagation speed in pure opening Mode I, in Plexiglas, deduced from experiments carried out with Slotted Double-Cantilever Beam (SDCB) specimens.

Figure 8 shows the calculated strain energy release rate of the branch crack (normalized by G_0) as a function of the length of the branch crack L (normalized by the half-length a of the initial slot) for the compressive applied stress $\sigma = 35$ MPa and two other near stresses 30 and 40 MPa. The representative curve of the applied stress ($\sigma = 35$ MPa) intersects the equilibrium curve $G = G_0$ for the length $L_0 = 44\,\mu$m, which is slightly greater than the size of microcracks at the edge of the open slot induced by the sawing method. But as L_0 is smaller than L_c, i.e. $(\partial G/\partial L)_\sigma > 0$, it is not surprising that the branch crack propagates at increasing speed (Fig. 5). The corresponding experimental points are represented by diamonds in Fig. 8; each point is obtained by associating to a length L the corresponding crack speed $v = dL/dt$, deduced from Fig. 6, and the associated strain energy release rate deduced from Fig. 7. During the stage of spontaneous subcritical crack growth, the data (diamonds in Fig. 8) fall in the immediate vicinity of the curve $\sigma = 35$ MPa. This curve intersects the horizontal $G = G_c$ for $L_1' = 1.25$ mm that exactly corresponds to the experimental value L_1 (Fig. 6) and $L_2' = 3.15$ mm which is slightly greater than the experimental value $L_2 = 2.5$ mm. These two values L_1' and L_2' delimit the propagation corresponding to the velocity jump and this agrees well with the experimental data. Then G decreases with increasing length L, because $(\partial G/\partial L)_\sigma < 0$, and the corresponding data, which characterize the controllable subcritical crack growth stage (circles in Fig. 8), again remain in the immediate vicinity of the applied stress curve $\sigma = 35$ MPa.

BIAXIAL LOADING CONDITIONS

In a few experiments Plexiglas plates were submitted to biaxial loading with minor lateral/axial stress ratio k of around 1/10. It was shown that the branch crack propagation was inhibited, whereas a shear band developed (associated with en échelon shallow cracks in the presence of ethyl alcohol) and spread roughly along the continuation of the slot. This case is illustrated in Fig. 2(b) for the same axial compressive stress as in Fig. 2(a) with a lateral/axial stress ratio of $k = 10\%$. Figure 9 showing the stress field around an elliptical defect at

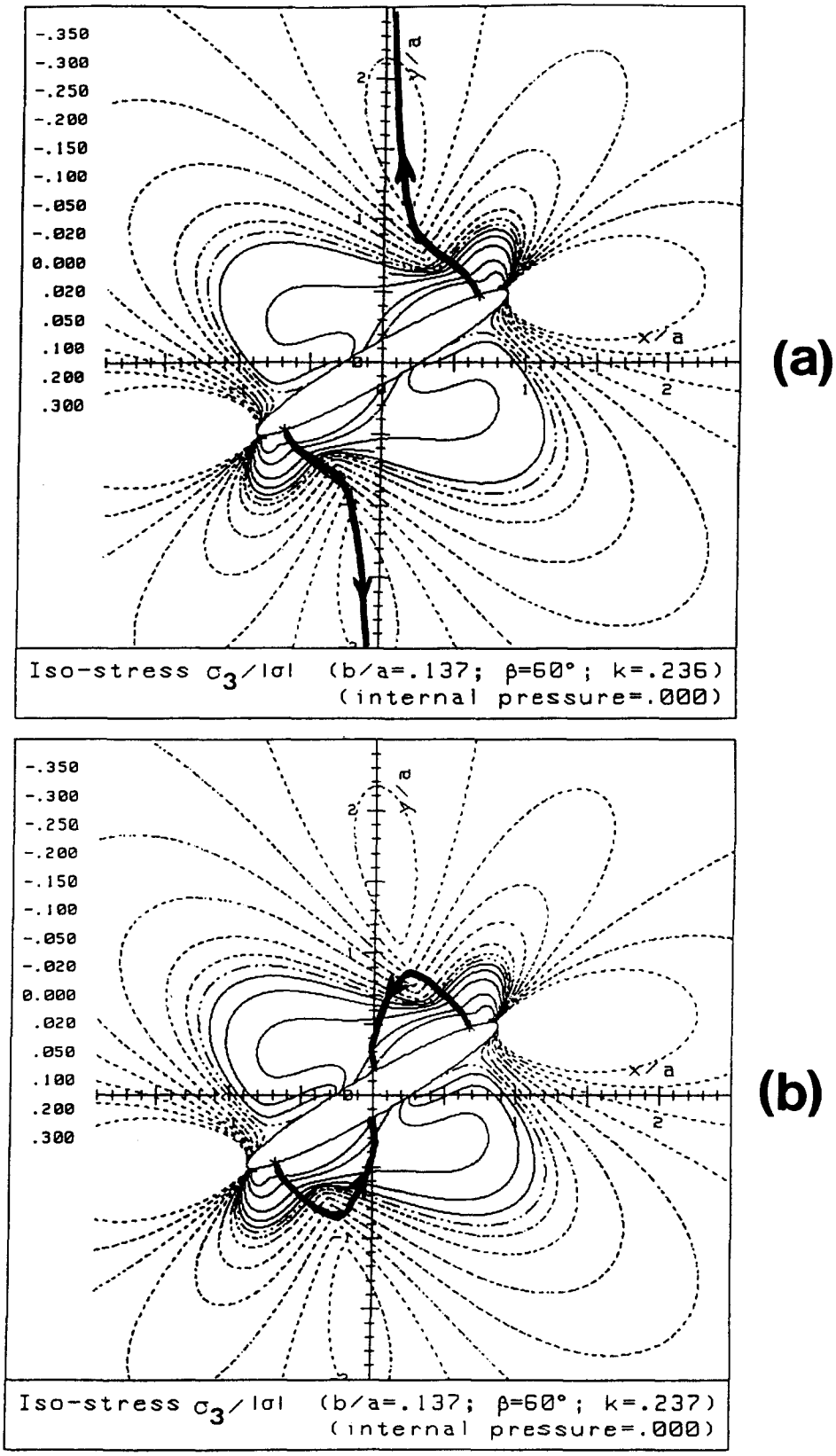

Fig. 9. Calculated contours of the principal stress σ_3 around an elliptical slot ($b/a = 0.137$) inclined at $\beta = 60°$ to the major loading axis, with two very closely related values of lateral confinement: (a) 23.6% and (b) 23.7%. The stress trajectories (thick lines) of σ_1 passing through the point where σ_3 is maximum at the edge of the elliptical slot are superimposed. Presentation of the contours is the same as in Fig. 4.

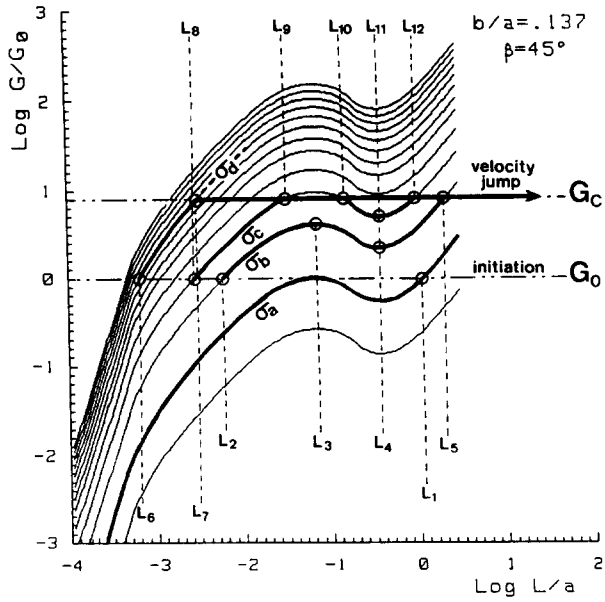

Fig. 10. Calculated variations of the strain energy release rate G as a function of the length L of the branch crack (both normalized as in Fig. 5), showing the influence of internal pressure in uniaxial loading conditions. The variation is calculated along the same σ_1 trajectory as in Fig. 5. The different curves correspond to various uniaxial applied compressive stress σ (normalized to σ_0) with internal pressure equal to 0.4 σ ($\beta = 45°$, $a = 5$ mm, $R = 150\,\mu$m).

$\beta = 60°$ submitted to biaxial loading illustrates a way of inhibiting propagation: from $k = 0.236$ to $k = 0.237$ the σ_1 trajectory featuring the propagation path evolves from the classical position (a) to an atypical curling position (b) which cannot correspond to any real path. The analysis also predicts that the threshold ratio k should directly depend on β.

INFLUENCE OF AN INTERNAL PRESSURE

As shown above, the experimental results agree very well with the theoretical models. Now we study the stress field around a pre-existing slot with internal pressure, in order to examine its influence on the kinetics of branching through $G(L)$ curves. The stress field is obtained by a classical superimposition of the stress field due to the external uniaxial or biaxial loading on to the stress field due to uniform traction at the infinity (far field traction) applied to the same elliptical defect. As soon as the internal pressure is applied, $G(L)$ curves which predict the propagation regimes have a very different shape from those corresponding to uniaxial or biaxial loading without internal pressure (Fig. 5). Figure 10 shows this for internal pressures of 40% of the external uniaxial normalized compressive stress and for various values of the latter. These $G(L)$ curves show three successive parts: a first part with positive slope leading to a maximum, a second one corresponding to a negative segment and third, a new positive segment. The question of whether the latter could be preluding another maximum (thus giving a bimodal curve as for internal pressure of 40%) remains unsolved; but if it exists, this maximum would obviously be higher than the previous one.

The prediction of the propagation regimes follows that already discussed for Fig. 5, but with specific aspects linked to the particular shape of the $G(L)$ curves.

(1) If the given external load does not exceed the threshold value σ_a, no branching occurs (Fig. 2b). Strictly speaking, branching could initiate from a fracture of length L_1 but as this dimension is nearly equivalent to half the length of the initial slot, this case is of limited interest.

(2) With a moderate external load σ_b, branching may initiate from a microcrack of length L_2 whose propagation occurs in three successive regimes: spontaneous (increasing speed) from L_2 to L_3, controllable (decreasing speed) from L_3 to L_4 and then spontaneous again from L_4 to L_5: this precedes a velocity jump (catastrophic propagation) from L_5. This velocity jump produces a branch crack whose final length is at least equal to 10^3 times the initial length L_2.

(3) With a high load σ_d very small microcracks can lead to branching. In this case a microcrack of length L_6 propagates spontaneously up to L_7, which would remain a very small crack with respect to the initial defect if the unavoidable velocity jump did not occur. The greater the applied stress, the smaller the microcrack producing a branch crack and the greater the velocity jump. For σ_d the length L_6 of the initial microcrack is multiplied at least by 10^4.

(4) The situation between 2 and 3 is particularly interesting, for it was observed in the course of preliminary experiments on Plexiglas plates. With applied stress σ_c, a microcrack of length L_8 situated at the most favourable point of the slot edge (maximum σ_3 tensile stress concentrations) gives a branch crack with a stable and spontaneous propagation from L_8 to L_9. After a first velocity jump which increases spontaneously from L_9 to L_{10}, a new stable propagation phase appears, first controllable from L_{10} to L_{11} and then spontaneous from L_{11} to L_{12} before a new velocity jump occurs as soon as length L_{12} is reached.

This helps us to understand how small defects or cracks can propagate out of proportion to their initial size. Such propagation could be due to a unique velocity jump; or it may correspond to the succession of the first velocity jump of very limited extension and another starting from a much longer branch as the two jumps are separated by a phase of slower lengthening.

SUPERIMPOSITION OF BIAXIAL LOADING AND INTERNAL PRESSURE

It is of geological importance to be able to predict branching behaviour from a pre-existing slot submitted to biaxial loading with internal fluid pressure. We limit the discussion to the case illustrated in Fig. 11, where internal pressure is increased from 0 to 100% of the value of the major (axial) applied compressive stress under biaxial loading conditions, with k = minor

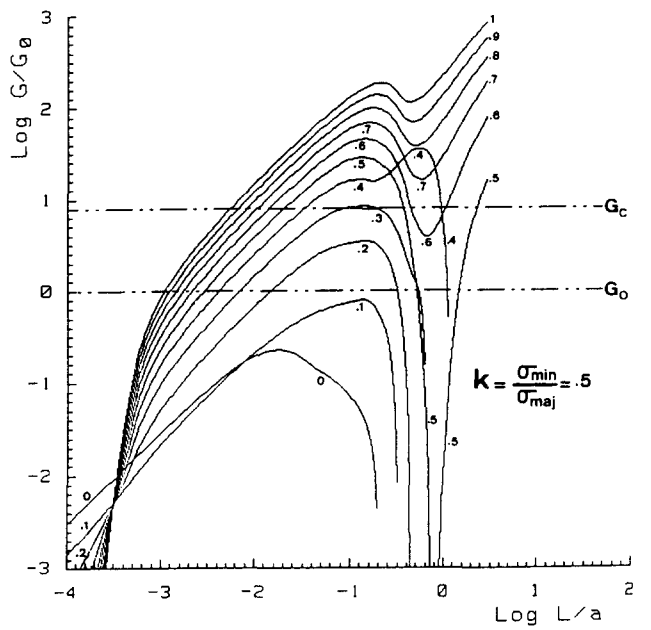

Fig. 11. Calculated variations of the strain energy release rate G (normalized by the strain energy release rate G_0 at zero crack propagation speed) as a function of the length L of the branch crack (normalized by the half-crack length a) along the stress trajectory of σ_1 touching the point of maximum tensile stress σ_3 at the edge of the slot, for a minor stress equal to half the major stress, and various values of internal pressure ($\beta = 45°$, $a = 5$ mm, $R = 150\ \mu$m).

(lateral) / major (axial) applied compressive stress ratio = 0.5.

This shows that no propagation can be expected for an internal pressure of less than 12% of the main applied compressive stress. For 20%, the unimodal curve indicates subcritical crack growth with slight increase in the branch crack. This behaviour with a small velocity jump is still present for 30%. For 40% a true bimodal curve occurs, but with a single velocity jump leading to a branch length about half the length of the defect. A velocity jump leading to large extension of pre-existing microfractures can only be observed when the internal pressure is well over 50%; i.e. when the internal pressure slightly exceeds the lateral stress. For 60% internal pressure, there will be continuous propagation with two velocity jumps as already shown in Fig. 10 for σ_c. Obviously 50% (i.e. internal pressure = lateral stress) is a critical point for which the propagation should stop after the first velocity jump, but a slight increase in internal pressure or a very slight decrease in k could trigger off a second velocity jump with very great increase in length. It is evident that for a velocity jump which produces a large extension, the initial microcrack is very small (about 1/1000 of the final length) and thus could correspond to relatively very small flaws in geological materials.

IMPLICATIONS AND CONCLUSION

The aim of this paper is to provide some basis for a physical approach to branch fractures, and especially their kinetics. Geological applications are varied, needing more detailed discussion in a separate paper. Potential applications concern isolated branching features stemming from macroscopic oblique defects such as joints, dikes, veins and solution surfaces. Though scarce, the natural features closely resembling the model are very important, such as the fault–stylolite–tension gash system described by Rispoli (1981) (Fig. 1a). Obviously as friction is not taken into account in the model, the corresponding stress field cannot be applied as it is. In particular, the predicted orthogonality of branching is only observed in the case of the reactivation of fractures where internal pressure prevents any contact between the walls (Fig. 1b). Another hindrance to direct application is that geological observations do not at present allow us to check whether the movement is perpendicular to the defect front, or whether the section in question is perpendicular to the defect and parallel to the movement. Statistically, most of the described branching features must correspond to mixed-mode situations (II + III) cross-cut by observation planes of unknown orientation with respect to the movement. This could be one reason for the wide variety of features observed.

A more direct application deals with the interpretation of fractographic features observed on Mode I rupture joint walls which indicate speed variations. It is well established that these joints are initiated from defects (Pollard & Aydin 1988) and that internal pressure is often superimposed on the least tectonic stress to determine propagation (Secor 1965). The model could be developed to take into account variation in k and internal pressure during incipient propagation; other fluctuations in speed during this stage might be found by examining experimental and natural fractographic features. Finally the model is important for seismic phenomena: the velocity jump on branch features could give some tensile seismic sources (non-double couple sources), as inferred by Sileny *et al.* (1986). Some aftershock distributions seem to appear in situations comparable to branching. The important point is that the model gives some idea of how catastrophic phenomena in rupture can be triggered off from very minute cracks on the defect, whose position and length are impossible to observe in experimental and *a fortiori* in natural conditions, or from very slight variations in the applied stress and/or internal pressure. In particular, this is because the model takes into account the difference between the strain energy release rate value at equilibrium, and the critical G_c value corresponding to catastrophic propagation; this is not often included in papers dealing with natural fracture propagation mechanisms. This difference emphasizes the importance of subcritical propagations over long periods, which should not be neglected in geological contexts.

REFERENCES

Ashby, M. F. & Hallam, S. D. 1986. The failure of brittle solids containing small cracks under compressive stress states. *Acta metall.* **34**, 497–510.

Barquins, M., Ghalayini, K. & Petit, J.-P. 1989a. Branchement de

fissures sous compression uniaxiale. *C. r. Acad. Sci., Paris, Sér.* II **308**, 899–905.

Barquins, M., Ghalayini, K., Maugis, D. & Petit J.-P. 1989b. Cinétique de propagation des fissures branchées sous compression uniaxiale. *C. r. Acad. Sci., Paris, Sér.* II **309**, 1451–1456.

Barquins, M., Petit, J.-P., Maugis, D. & Ghalayini, K. In press. Paths and kinetics of branching from defects under uniaxial and biaxial compressive loading. *Int. J. Fract.*

Brace, W. F. & Bombolakis, E. G. 1963. A note on brittle crack growth in compression. *J. geophys. Res.* **68**, 3709–3713.

Cottrell, B. 1972. Brittle fracture in compression. *Int J. Fracture Mech.* **8**, 195–208.

Engelder, T. & Lacazette, A. 1990. Natural hydraulic fracturing. In: *Rock Joints* (edited by Barton, N. & Stephansson, O.). Balkema, Rotterdam, 35–43.

Granier, T. 1985. Origin, damping and pattern of development of faults in granite. *Tectonics* **4**, 721–737.

Inglis, C. E. 1913. Stress in a plate due to the presence of cracks and sharp corners. *Trans. Inst. Naval. Archit.* **55**, 219–224.

Hoek, E. & Bienawsky, Z. T. 1965. Brittle fracture propagation in rocks under compression. *Int. J. Fracture Mech.* **1**, 137–155.

Lajtai, E. Z. 1971. A theoretical and experimental evaluation of the Griffith theory of brittle fracture. *Tectonophysics* **11**, 129–156.

Lawn, B. R. & Wilshaw, T. R. 1975. *Fracture of Brittle Solids.* Cambridge University Press, Cambridge.

Mouginot, R. & Maugis, D. 1985. Fracture indentation beneath flat and spherical punches. *J. Mater. Sci.* **20**, 4354–4376.

Muskhelishvili, N. I. 1975. *Some Basic Problems of the Mathematical Theory of Elasticity.* Noordhoff, Leyden.

Nemat-Nasser, S. & Horii, H. 1982. Compression-induced nonplanar crack extension with application to splitting, exfoliation and rockburst. *J. geophys Res.* **87**, 6805–6821.

Paris, P. C. & Sih, G. S. 1965. Stress analysis of cracks. In: *Fracture Toughness Testing and its Applications. Spec. Tech. Publ. Am. Soc. Testing Materials* **381**, 30–83.

Petit, J.-P. & Barquins, M. 1987. Formation de fissures en milieu confiné dans le PMMA: modèle analogique de formation de structures tectoniques cassantes. *C. r. Acad. Sci., Paris, Sér.* II **305**, 55–60.

Petit, J.-P. & Barquins, M. 1988. Can natural faults propagate under Mode II conditions? *Tectonics* **7**, 1243–1256.

Pollard, D. D. 1973. Derivation and evaluation of a mechanical model for sheet intrusions. *Tectonophysics* **19**, 233–269.

Pollard, D. D. & Aydin, A. 1988. Progress in understanding jointing over the past century. *Bull. geol. Soc. Am.* **100**, 1181–1204.

Pollard, D. D. & Segall, P. 1987. Theoretical displacements and stress near fractures in rocks: with implications to faults, joints, veins, dikes, and solution surfaces. In: *Fracture Mechanics of Rocks* (edited by Atkinson, B. K.). Academic Press, London, 277–347.

Rispoli, R. 1981. Stress field about strike-slip faults from stylolites and tension gashes. *Tectonophysics* **75**, T29–T36.

Rudnicki, J. W. 1977. The inception of faulting in a rock mass with a weakened zone. *J. geophys. Res.* **82**, 844–854.

Secor, D. T. 1965. Role of fluid pressure in jointing. *Am J. Sci.* **263**, 633–646.

Sibson, R. H. 1990. Conditions for fault valve behaviour. In: *Deformation Mechanisms, Rheology and Tectonics* (edited by Knipe, R. J. & Rutter, E. H.). *Spec. Publs. geol. Soc. Lond.* **54**, 15–28.

Sileny, J., Ritsema, A. R., Csikos, I. & Kozak, J. 1986. Do some shallow earthquakes have a tensile source component? *Pure & Appl. Geophys.* **124**, 825–840.

Sketty, D. K., Rosenfeld, A. R. & Duckworth, W. H. 1987. Mixed mode fracture in biaxial stress state: Application to the diametral compression test. *Engng Fracture Mech.* **26**, 825–840.

Williams, J. G. 1972. Viscoelastic and thermal effects on crack growth in PMMA. *Int. J. Fracture Mech.* **8**, 393–401.

Wu, H.-C. & Chang, K.-J. 1978. Angled elliptic notch problem in compression and tension. *J. Appl. Mech.* **45**, 258–262.